Buoyancy-driven convection around chemical fronts traveling in covered horizontal solution layers

L. Rongy
Nonlinear Physical Chemistry Unit and Center for Nonlinear Phenomena and Complex Systems, CP 231, Université Libre de Bruxelles (ULB), 1050 Brussels, Belgium

N. Goyal and E. Meiburg
Department of Mechanical Engineering, University of California, Santa Barbara, California 93106, USA

A. De Wit
Nonlinear Physical Chemistry Unit and Center for Nonlinear Phenomena and Complex Systems, CP 231, Université Libre de Bruxelles (ULB), 1050 Brussels, Belgium

(Received 13 April 2007; accepted 3 July 2007; published online 21 September 2007)

Density differences across an autocatalytic chemical front traveling horizontally in covered thin layers of solution trigger hydrodynamic flows which can alter the concentration profile. We theoretically investigate the spatiotemporal evolution and asymptotic dynamics resulting from such an interplay between isothermal chemical reactions, diffusion, and buoyancy-driven convection. The studied model couples the reaction-diffusion-convection evolution equation for the concentration of an autocatalytic species to the incompressible Stokes equations ruling the evolution of the flow velocity in a two-dimensional geometry. The dimensionless parameter of the problem is a solutal Rayleigh number constructed upon the characteristic reaction-diffusion length scale. We show numerically that the asymptotic dynamics is one steady vortex surrounding, deforming, and accelerating the chemical front. This chemohydrodynamic structure propagating at a constant speed is quite different from the one obtained in the case of a pure hydrodynamic flow resulting from the contact between two solutions of different density or from the pure reaction-diffusion planar traveling front. The dynamics is symmetric with regard to the middle of the layer thickness for positive and negative Rayleigh numbers corresponding to products, respectively, lighter or heavier than the reactants. A parametric study shows that the intensity of the flow, the propagation speed, and the deformation of the front are increasing functions of the Rayleigh number and of the layer thickness. In particular, the asymptotic mixing length and reaction-diffusion-convection speed both scale as $\sqrt{\mathrm{Ra}}$ for $\mathrm{Ra}>5$. The velocity and concentration fields in the asymptotic dynamics are also found to exhibit self-similar properties with Ra. A comparison of the dynamics in the case of a monostable versus bistable kinetics is provided. Good agreement is obtained with experimental data on the speed of iodate-arsenous acid fronts propagating in horizontal capillaries. We furthermore compare the buoyancy-driven dynamics studied here to Marangoni-driven deformation of traveling chemical fronts in solution open to the air in the absence of gravity previously studied in the same geometry [L. Rongy and A. De Wit, J. Chem. Phys. **124**, 164705 (2006)]. © *2007 American Institute of Physics*. [DOI: 10.1063/1.2766956]

I. INTRODUCTION

In the absence of gels, horizontal propagation of autocatalytic chemical fronts in thin solution layers open to the air can be affected by buoyancy and Marangoni-driven flows due to gradients of concentration across the front which can trigger gradients in density and/or surface tension. These hydrodynamic flows can deform and accelerate the fronts as has already been shown experimentally and numerically in the past.[1–8] It remains, however, most often difficult to discriminate the relative influence of buoyancy- and surface-tension-driven flows in the complex dynamics of the system. In a previous theoretical study,[9,10] we have quantitatively analyzed the spatiotemporal dynamics of chemical fronts traveling horizontally in a thin solution layer open to the air when Marangoni forces are acting at the surface in the absence of gravity. We have characterized the asymptotic dynamics of the system as a function of the important parameters of the problem that are a Marangoni number and the thickness of the solution layer. It is the objective of this article to complement this previous study by analyzing quantitatively in a similar horizontal geometry the dynamics of isothermal chemical fronts when density differences due to compositional changes act across the front to trigger hydrodynamic flows in a closed system in the absence of interfacial Marangoni stresses.

Experimentally, numerous works have noted acceleration of fronts traveling in closed systems entirely filled with the solution. In this case, no interface with air exists and Marangoni flows are thus excluded. When the front travels parallel to the gravity field, hydrodynamic instabilities can lead to a cellular deformation of the initially planar interface

between reactants and products. This situation has been thoroughly analyzed both experimentally and theoretically in capillaries,[3,4,6,11–14] in spatially extended Hele-Shaw geometries,[15–18] and, more recently, in three-dimensional tanks.[19] In such a vertical orientation, hydrodynamic flows are due to Rayleigh-Taylor, Rayleigh-Bénard, double-diffusive, or even chemically driven instabilities.[20,21] Flows are triggered typically when the heavier solution lies on top of the lighter one or if double-diffusive effects due to the differential diffusivity of mass and heat are involved. Otherwise, the front remains planar and travels at a reaction-diffusion (RD) speed v as in a gel.

If the front travels horizontally, a density difference across the front will on the contrary always lead to hydrodynamic flows. In the absence of chemical reactions, it is known that a vertical interface between two miscible fluids of different densities cannot be maintained. Indeed, the heavier solution is naturally sinking below the lighter one triggering convection in the system. In the present geometry, the flow resulting under such conditions is called a lock-exchange gravity current.[22] This type of flow has been studied extensively due to its relevance in a wide range of geophysical and industrial contexts.[23] It is of interest to analyze to which extent a chemical reaction at the origin of the density difference across a self-sustained interface can modify this picture. In this respect, autocatalytic chemical fronts traveling in horizontal covered solution layers provide an instructive model system to gain insight into such a problem.

Experimental evidence has shown that autocatalytic fronts propagating in horizontal capillaries can travel faster than in gels[3,4,6,11,12,14] and be deformed by convection.[12,14] However, quantitative studies of the deformation and of the acceleration of the front as a function of the density difference across the front or as a function of the thickness of the layer are scarce.[11] From a theoretical point of view, numerical studies have provided examples of buoyancy-driven deformation of traveling pulses in excitable systems.[24–29] Vasquez *et al.*[30] have numerically shown that simple chemical fronts propagating horizontally in nonexcitable systems can be accelerated and deformed by the presence of a convective flow around the front. They find good agreement between their predicted reaction-diffusion-convection speed for iodate-arsenous acid fronts and values measured experimentally in thin capillary tubes. However, no quantitative analysis of the flow properties and of the front deformation is provided.

In this context, our objective is to quantify theoretically in detail to what extent buoyancy effects due to a density difference across an isothermal chemical front traveling horizontally in the absence of any Marangoni flows triggers the presence of a convection roll. We study quantitatively how this flow deforms the front and accelerates it with regard to the pure reaction-diffusion case. To do so, we numerically integrate in a two-dimensional geometry the incompressible Stokes equations for the velocity field coupled through a buoyancy term characterized by a dimensionless Rayleigh number to a reaction-diffusion-convection (RDC) equation for the concentration c of the product of a monostable autocatalytic reaction. The density of the solution is supposed to vary linearly with c. A parametric study reveals that the convective deformation of the front is symmetric with regard to the middle of the layer thickness depending on whether the products are heavier than the reactants or vice versa. The propagation speed and front deformation, as well as the intensity of the flow, are seen to increase with the layer thickness and with the density differences. The asymptotic dynamics also features interesting scalings and self-similar properties. A comparison is made of the dynamics in systems with, respectively, monostable and bistable kinetics. Comparison with experimental data available for the iodate-arsenous acid reaction[11] shows good agreement.

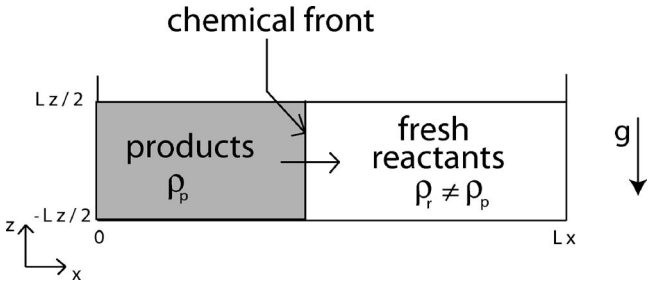

FIG. 1. Sketch of the system.

Our article is organized as follows: In Sec. II, we first introduce the geometry of the system and present our reaction-diffusion-convection model. The properties of the pure reaction-diffusion front are recalled and the numerical technique used to integrate our model is described. The results of our nonlinear simulations are presented and discussed in Sec. III before concluding in Sec. IV.

II. PHYSICAL PROBLEM AND NUMERICAL METHOD

A. Equations of motion

We consider a two-dimensional (2D) thin aqueous solution layer of length L_x and height L_z, corresponding to a vertical cut in a covered rectangular channel oriented horizontally in the gravity field $\underline{g}$ (see Fig. 1). An isothermal chemical front propagates along the x direction with the density of the products ρ_p different from that of the reactants ρ_r. This chemical front is the solution of a reaction-diffusion-convection equation (1) for the concentration c of the solute that determines the density $\rho(c)$ of the solution. The evolution of the 2D velocity field $\underline{v}=(u,w)$ is described by the incompressible Stokes equations [Eqs. (2) and (3)]. Namely,

$$\frac{\partial c}{\partial t} + \underline{v} \cdot \underline{\nabla} c = D\nabla^2 c + f(c), \tag{1}$$

$$\underline{\nabla} p = \mu \nabla^2 \underline{v} + \rho(c)\underline{g}, \tag{2}$$

$$\mathrm{div}\ \underline{v} = 0, \tag{3}$$

where p denotes the pressure and $\underline{g}=(0,-g)$ is the gravity acceleration acting along z. The molecular diffusion coefficient D and the dynamic viscosity μ are assumed to be constant. The chemical production term $f(c)=kc^2(a_0-c)$ is chosen here as a simple one-variable cubic kinetics modeling a typical autocatalytic reaction where k is the rate constant and

a_0 is the initial reactant concentration. This kinetics is capable of sustaining traveling fronts between two different states when coupled to molecular diffusion and describes chemical systems such as the iodate-arsenous acid redox reaction in a given range of concentrations.[31–33] We have used the Boussinesq approximation assuming that small changes in density are negligible except in the buoyancy term $\rho \underline{g}$ of Eq. (2).

The dimensionless equations are obtained by using the characteristic scales of the reaction-diffusion system: for time, $\tau_c = 1/ka_0^2$, for length, $L_c = \sqrt{D\tau_c}$, for velocity, $U_c = L_c/\tau_c = \sqrt{D/\tau_c}$, and for concentration, a_0. The pressure is scaled by $p_c = \mu/\tau_c$, so that the dimensionless pressure $p' = p/p_c$. In addition, we define a hydrostatic pressure gradient as $\nabla p'' = \nabla p' - \rho_r L_c \underline{g}/p_c$, which is used in Eq. (5) where the primes have been dropped. Incorporating a linear dependence between the density and the product concentration, $\rho(c) = \rho_r + (d\rho/dc)c$ with ρ_r the density of the reactant solution corresponding to $c=0$, we obtain the dimensionless governing equations

$$\frac{\partial c}{\partial t} + \underline{v} \cdot \underline{\nabla} c = \nabla^2 c + c^2(1-c), \tag{4}$$

$$\underline{\nabla} p = \nabla^2 \underline{v} + \mathrm{Ra}\, c \underline{i}_z, \tag{5}$$

$$\mathrm{div}\, \underline{v} = 0, \tag{6}$$

where Ra is the dimensionless Rayleigh number defined as

$$\mathrm{Ra} = -\frac{d\rho}{dc}\frac{a_0 L_c^3 g}{D\mu}. \tag{7}$$

The Rayleigh number is positive if the product decreases the density and negative otherwise. It quantifies the coupling strength between the reaction-diffusion processes and the convective motions and is therefore one of the important parameters of our model. At each boundary of the domain we require zero-flux boundary conditions for the chemical concentration c. The hydrodynamic boundary conditions are rigid walls with no slip for the vertical boundaries and slip walls for the horizontal boundaries

$$\frac{\partial c}{\partial x} = u = \frac{\partial w}{\partial x} = 0 \quad \text{at } x = 0, \quad x = L_x, \tag{8}$$

$$\frac{\partial c}{\partial z} = u = w = 0 \quad \text{at } z = -L_z/2, \quad z = L_z/2, \tag{9}$$

where L_x and L_z now represent, respectively, the dimensionless length and height of the layer. The length of the system and slip walls do not influence the results as long as it is taken sufficiently long for the front not to interact with a lateral boundary on the time of interest. On the other hand, the layer thickness L_z is the second important parameter of our model and will be varied along with the Rayleigh number.

In Sec. III we perform the numerical integration of the dimensionless model (4)–(9) in order to characterize the hydrodynamic motions initiated by the density gradients across the front and quantify their influence on this RD front dynamics. In this framework, let us first recall the properties of such a front in the absence of flow.

B. Reaction-diffusion front

In the absence of flow, i.e., for a Rayleigh number equal to zero, the RD equation (4) with $\underline{v}=0$ allows exact integration and admits as solution the following propagating front:[31–33]

$$c(x,t) = \frac{1}{1+e^{(x-vt)/\sqrt{2}}} = \frac{1}{2}\left[1 + \tanh\left(-\frac{\sqrt{2}}{4}(x-vt)\right)\right], \tag{10}$$

where $v = \sqrt{2}/2$ is the constant RD speed of the front. This profile connects the kinetically stable product steady state $c=1$ to the invaded $c=0$ solution corresponding to the marginally stable reactants. The width w_{RD} of this front, arbitrarily defined as the distance between $c=0.99$ and $c=0.01$, equals $w_{\mathrm{RD}} = 2\sqrt{2}\ln 99 \approx 13$. This definition has the advantage to allow for an easy study of the possible deformation in time of the front by a simple tracking of the $c=0.01$ and $c=0.99$ isoconcentration lines.

C. Numerical method and validation studies

Nonlinear Stokes flow simulations are employed to numerically integrate Eqs. (4)–(9). For this purpose, we cast the two-dimensional Stokes equations into a fourth order stream function formulation by taking the curl of the momentum equations and replacing the velocity terms by the stream function and its derivatives. We arrive at

$$\nabla^4 \psi = \mathrm{Ra}\frac{\partial c}{\partial x}, \tag{11}$$

$$\frac{\partial c}{\partial t} + \underline{v} \cdot \underline{\nabla} c = \nabla^2 c + c^2(1-c), \tag{12}$$

where the stream function ψ is defined by

$$u = \frac{\partial \psi}{\partial z}, \quad w = -\frac{\partial \psi}{\partial x} \tag{13}$$

and

$$\nabla^4 \psi = \frac{\partial^4 \psi}{\partial x^4} + 2\frac{\partial^4 \psi}{\partial x^2 z^2} + \frac{\partial^4 \psi}{\partial z^4}. \tag{14}$$

Figure 1 shows the two-dimensional computational domain employed for the simulations. We select the size of the domain in the front propagation direction sufficiently large, so that the front can evolve without being affected by the upstream and downstream boundaries. The boundary conditions, in Eqs. (8) and (9), take the following form in terms of the new variables

$$\psi = \frac{\partial^2 \psi}{\partial x^2} = \frac{\partial c}{\partial x} = 0 \quad \text{at } x = 0, \quad x = L_x \tag{15}$$

$$\psi = \frac{\partial \psi}{\partial z} = \frac{\partial c}{\partial z} = 0 \quad \text{at } z = -L_z/2, \quad z = L_z/2. \tag{16}$$

The simulations are started with the fluid initially at rest and a one-dimensional concentration profile which describes the convectionless RD profile (10) discussed above.

An equidistant computational grid is employed in both directions. The temporal discretization is accomplished by an explicit third order accurate, low-storage Runge-Kutta time integration scheme[34] for updating the concentration field. Sixth order accurate central compact finite differences[35] are employed for the spatial discretization of the concentration derivatives in both directions, in order to avoid the appearance of numerical instabilities in the reaction-diffusion-convection equation. The zero-flux boundary conditions prescribed for the concentration field at all ends of the domain impose symmetry conditions on the concentration field about all the boundaries, so that the sixth order differencing scheme can be extended to the boundaries. Since an explicit time marching scheme is used for the species equation, the boundary conditions are easily implemented during evaluation of the concentration derivatives by the compact finite differencing scheme. Spatial derivatives for the stream function are evaluated spectrally in the horizontal direction, using a sine series expansion[36,37] to represent the stream function variable. This methodology automatically implements the boundary conditions in the front propagation direction. In the vertical direction fourth order central compact finite differences are used to discretize the stream function equation. Similar to the concentration field, symmetry of the stream function at the top and bottom walls based on the Neumann boundary condition along with the prescription of $\psi=0$ enables us to extend this fourth order scheme to the boundaries while implementing the no-slip boundary conditions. Hence the solution of the discretized stream function equation reduces to solving a one-dimensional pentadiagonal system in the vertical direction for each Fourier mode in the streamwise direction. This is accomplished by a direct solution of the linear system using a pentadiagonal version of the well known Thomas algorithm.[38] The numerical code is parallelized on a distributed memory architecture using the message passing interface.

We examined the influence of the domain length and spatial resolution on our results, in order to ensure the absence of any numerical artifacts in our simulation results with regard to the detailed shape of the front and its propagation velocity. The largest simulations involved a computational domain of horizontal length 520 and height 20, with 1024×128 grid points. We applied our nonlinear simulation procedure to calculate the growth rates of gravity-driven instabilities in miscible Hele-Shaw flows in the absence of any chemical reaction, for which we had derived linear stability results in a previous investigation.[39] Excellent agreement between these two cases validated our numerical results for the hydrodynamic part. Concerning the chemical kinetics, we recover numerically the planar traveling front (10) with the correct RD speed $v=\sqrt{2}/2$ and width $w_{\mathrm{RD}} \approx 13$ when the Rayleigh number Ra is equal to zero.

FIG. 2. Propagation of a chemical front in the presence of chemically induced buoyancy convection for Ra=100, shown from top to bottom from $t=0$ up to $t=50$ with a time interval of $\Delta t=5$. The aspect ratio between $L_x=450$ and $L_z=10$ is preserved.

III. 2D BUOYANCY-DRIVEN FLOW AROUND CHEMICAL FRONTS: NONLINEAR DYNAMICS

In this section, we present the results of the numerical integration of Eqs. (4)–(9) with an initial condition corresponding to the traveling RD front described in Sec. II B and we investigate the influences of the Rayleigh number, of the layer thickness, and of the reaction kinetics on the nonlinear dynamics.

Let us first analyze the spatiotemporal dynamics of the system for a positive Ra for which the density decreases during the reaction. The reactants ahead of the front are thus heavier than the products and will naturally sink below them when the front travels horizontally in the gravity field. This is indeed what is observed, as shown in Fig. 2 which presents the evolution of the system for increasing time. The dynamics is represented by two-dimensional density plots of the product concentration ranging from $c=0$ (white) to $c=1$ (black). After a given transient during which convection due to the density difference sets in, the dynamics asymptotes to one convection roll turning clockwise, surrounding the front traveling here to the right and deforming it. Details of the flow around the front can be visualized in Fig. 3(a). The dynamics is quite different from the pure hydrodynamic situation in which a density difference across a vertical interface between two miscible fluids leads to convective mixing of the fluids until a homogeneous solution of density equal to the averaged value of the densities of two initially separated fluids is obtained in the reactor. Chemistry changes this situation drastically by providing a self-sustained moving interface which entrains the flow vortex at a constant speed and prevents it from extending until the boundaries and from mixing the two solutions.

A nonlinear simulation in the same geometry and same monostable kinetics as for Figs. 2 and 3(a), but now with a negative Ra of same magnitude, i.e., with the products heavier than the reactants, yields a vortex rotating now counterclockwise and propagating at the same speed to the right as the vortex for positive Ra. The concentration and flow fields are symmetric with regard to the axis $z=0$ of the positive Ra situation [see Fig. 3(b)]. This is logical as the density gradient across the front is just of opposite sign for positive and negative Rayleigh numbers of same amplitude. This is analogous to symmetric convective dynamics for $\mathrm{Ra}>0$ and $\mathrm{Ra}<0$ featuring two vortices around pulses in excitable systems.[25] It is thus sufficient in the remainder of the article

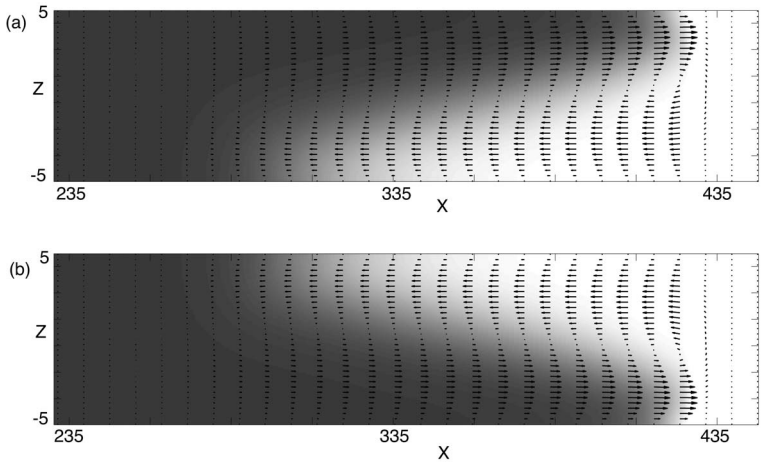

FIG. 3. Focus on the asymptotic convection roll traveling with the deformed front for Ra=100 (a) and Ra=−100 (b). The z direction has been magnified in order to see the details of the velocity field.

to study the parametric dependence of the dynamics around fronts for positive Ra, the situation with negative Ra being straightforwardly obtained by symmetry. Let us now analyze the influence of the magnitude of the Rayleigh number on the dynamics while keeping the layer thickness constant to $L_z=10$. This would correspond to a quite thin layer of the order of the typical RD width of a chemical front which is typically 1 mm in thickness.

A. Influence of the Rayleigh number

When Ra increases, the density difference across the front increases and the source of buoyancy flows is therefore more important. Hence the flow becomes more intensive and the deformation of the front more pronounced. This can be quantified by inspecting the mixing length of the front defined as the distance between $\langle c(x,t)\rangle=0.01$ and $\langle c(x,t)\rangle=0.99$ corresponding, respectively, to the tip and rear of the transversed averaged profile

$$\langle c(x,t)\rangle = \frac{1}{L_z}\int_{-L_z/2}^{L_z/2} c(x,z,t)dz. \tag{17}$$

As seen in Fig. 4(a), after a given transient during which convection develops, the mixing length saturates to a fixed value that we denote as W. The time needed to reach this asymptotic value W does not seem to depend on the Rayleigh number. A plot of W as a function of Ra [see Fig. 4(b)] shows that the asymptotic value of the mixing length is an increasing function of Ra which corresponds to an increased deformation of the front by convection when the density difference across the front increases. Note that $W=w_{\mathrm{RD}}$ for Ra=0, i.e., the mixing length is nothing else than the width of the reaction-diffusion front in the absence of flow. The dependence of the steady mixing length W on the Rayleigh number Ra can be fitted by a square root function, $W=15\sqrt{\mathrm{Ra}}$ for $\mathrm{Ra}\geqslant 5$. More intense convection for increasing Ra also leads to a more intense value of the constant asymptotic RDC speed V of the front along the x axis. This speed V plotted in Fig. 5(a) as a function of Ra has been obtained by measuring the slope of the position of the tip of the front as a function of time. When Ra=0, the RD speed v is recovered, while for $\mathrm{Ra}\geqslant 5$, the asymptotic propagation speed V is proportional to the square root of Ra: $V=0.79\sqrt{\mathrm{Ra}}$.

To characterize the convective motions initiated by the front propagation, we have plotted $u_{\max}$ the maximum absolute value of the asymptotic horizontal velocity u as a function of Ra in Fig. 5(b), showing that $u_{\max}$ increases like $0.96\sqrt{\mathrm{Ra}}$ for $\mathrm{Ra}\geqslant 30$. The maximum u intensity always corresponds to a positive u localized in the upper part of the layer for positive Ra (and in the lower part for negative Ra by symmetry). To compare the asymptotic dynamics when Ra increases, we have performed vertical cuts of the fluid

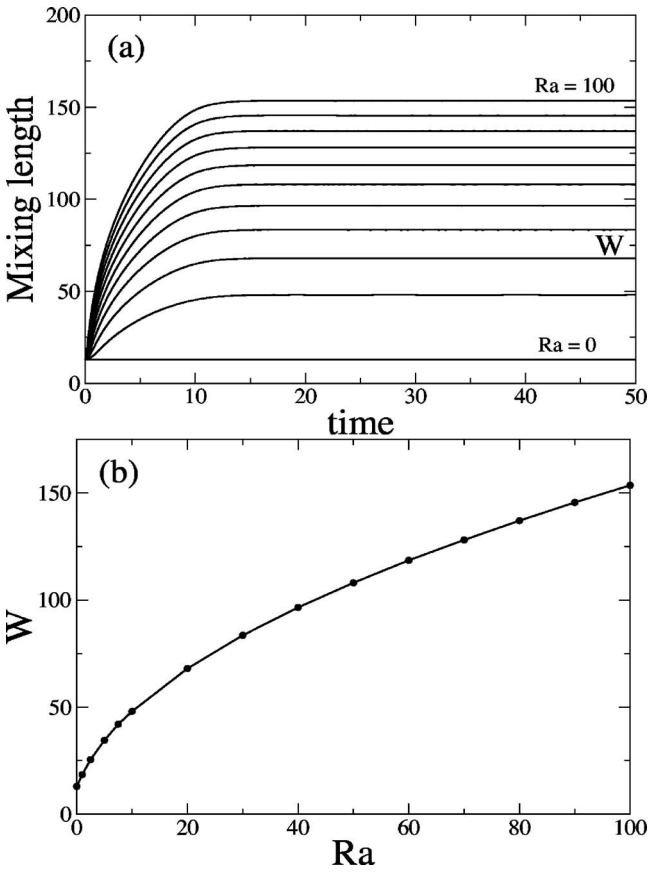

FIG. 4. Mixing lengths as a function of time for various increasing Rayleigh numbers between 0 and 100 with an interval of 10 between two successive curves (a) and asymptotic mixing length W as a function of the Rayleigh number (b).

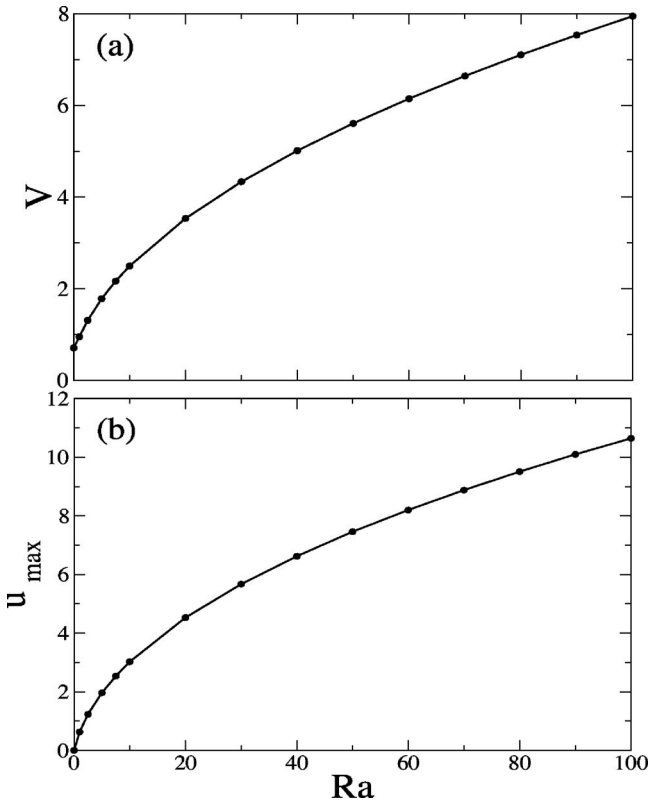

FIG. 5. Asymptotic propagation speed V (a) and maximum absolute value $u_{\max}$ of the asymptotic horizontal velocity u (b) as a function of the Rayleigh number.

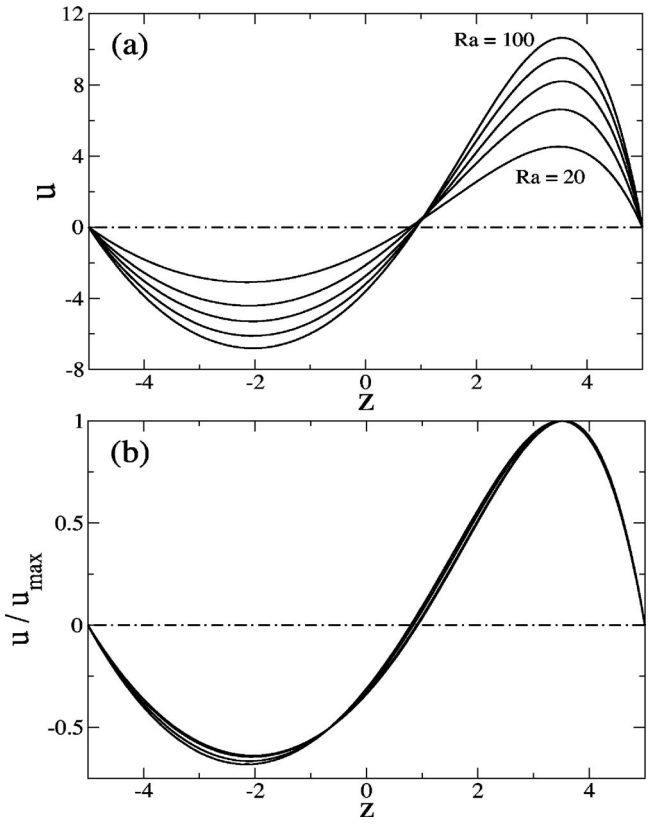

FIG. 6. (a) Asymptotic profiles of the horizontal fluid velocity u across the layer at $x_{\max}=x_{|u|=|u|_{\max}}$ for increasing Rayleigh numbers between 20 and 100 with an interval of 20 between two successive curves. The dot-dashed curve corresponds to Ra=0 when there is no convection. (b) Autosimilar profiles of the horizontal fluid velocity u renormalized with its maximum $u_{\max}$.

velocity u at the horizontal location $x_{\max}$ where u is maximum. Figure 6(a) shows thus $u(x_{\max},z)$ which has clearly all properties of a return flow with positive u in the upper layer of the system and negative u at the bottom. The intensity of this return flow increases with Ra while u is zero and gets its minimum and maximum values at the same positions along z for all the Rayleigh numbers. Indeed, the maximum value of u is always located around $6L_z/7$, at $z=3.52\pm dz$ (for $L_z=10$), where $u>0$ and is directed towards the reactants and dz is the numerical mesh size. This suggests an autosimilarity of the problem for different Rayleigh numbers which is clearly confirmed in Fig. 6(b) where we have normalized each curve of Fig. 6(a) with its maximum. We note that all the curves are then identical, with a better superposition when Ra increases. Note in Fig. 6(a) that the return flow is asymmetric across the layer, with a negative horizontal fluid velocity u at the middle of the layer, the position of zero u being shifted towards the surface. In fact, this position of zero u is a function of x which crosses $z=0$ at only one x near the center of the roll. At this point, the return flow is antisymmetric across the layer while it is asymmetric at any other x coordinate.

Finally, we have checked that the autosimilarity shown for u in Fig. 6(b) is also present in the asymptotic concentration profiles by comparing the asymptotic transversed averaged profiles $\langle c(x)\rangle$ for various Ra [see Fig. 7(a)]. If we rescale the mixing length of each profile to 1, all averaged profiles collapse on the same curve, the agreement improving when Ra increases [see Fig. 7(b)].

We can therefore conclude that the asymptotic regime reached when a propagating chemical front induces a 2D buoyancy-driven flow exhibits an autosimilarity when the density difference across the front, measured by the Rayleigh number Ra, changes. We have also shown in this section that increasing the convective motions by increasing Ra leads to a larger buoyancy-driven deformation W of the front which scales as $W\approx\sqrt{\mathrm{Ra}}$. The asymptotic autosimilar dynamics is a steady fluid vortex traveling with the front at a constant RDC speed V which also scales as $\sqrt{\mathrm{Ra}}$. Let us now fix the Rayleigh number to a constant positive value in order to analyze the influence of the layer thickness on the nonlinear dynamics.

B. Influence of the layer thickness

In this section, we fix the Rayleigh number to 20 and analyze the influence of variations of L_z $(4.0\leqslant L_z\leqslant 20.0)$. Indeed, considering the definition of the dimensionless Rayleigh number (7), we see that changes of Ra involve changes of the chemical parameters while it is much more easy in experiments to vary the layer thickness of the solution in a closed reactor.

When the layer thickness is modified, a steady regime is still reached. However, it takes longer for the system to reach it as L_z increases, since the flow has to develop in a larger thickness. This can be seen in Fig. 8 where we have plotted the temporal evolution of the mixing length for various val-

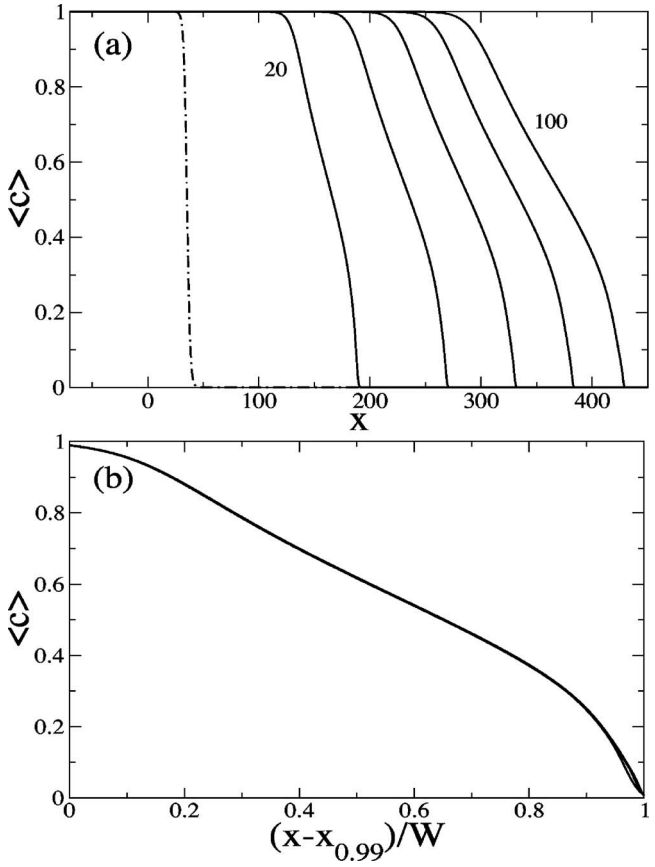

FIG. 7. (a) Asymptotic averaged concentration profiles $\langle c(x)\rangle$ for increasing Rayleigh numbers between 20 and 100 with an interval of 20 between two successive curves. The dot-dashed curve corresponds to the RD front for Ra=0 when there is no convection. (b) Autosimilar profiles of $\langle c\rangle$ as a function of the axial coordinate x rescaled with the mixing length between 0 and 1.

ues of L_z. The time taken to reach the asymptotic value W is an increasing function of L_z and corresponds to the time needed for the convection to set in. When the fluid layer thickness is increased, buoyancy convection is enhanced leading to a larger deformation of the front W, a larger propagation speed V, and more intense convection (see Fig. 9). The amplitude of the velocity field increases due probably to the fact that the system is less influenced by the no-slip

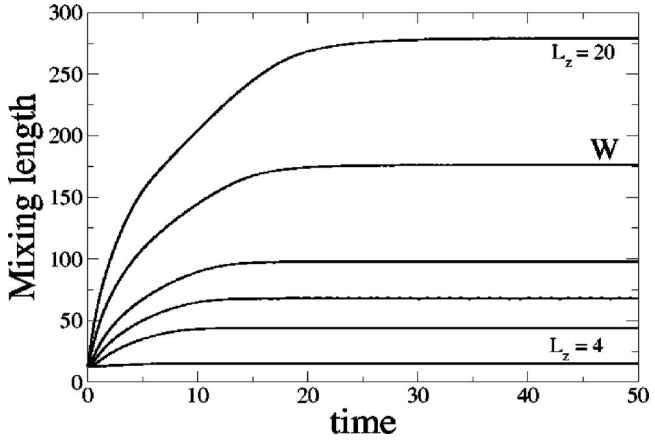

FIG. 8. Temporal evolution of the mixing length W for various values of the layer thickness, L_z=4;8;10;12;16;20 from bottom to top.

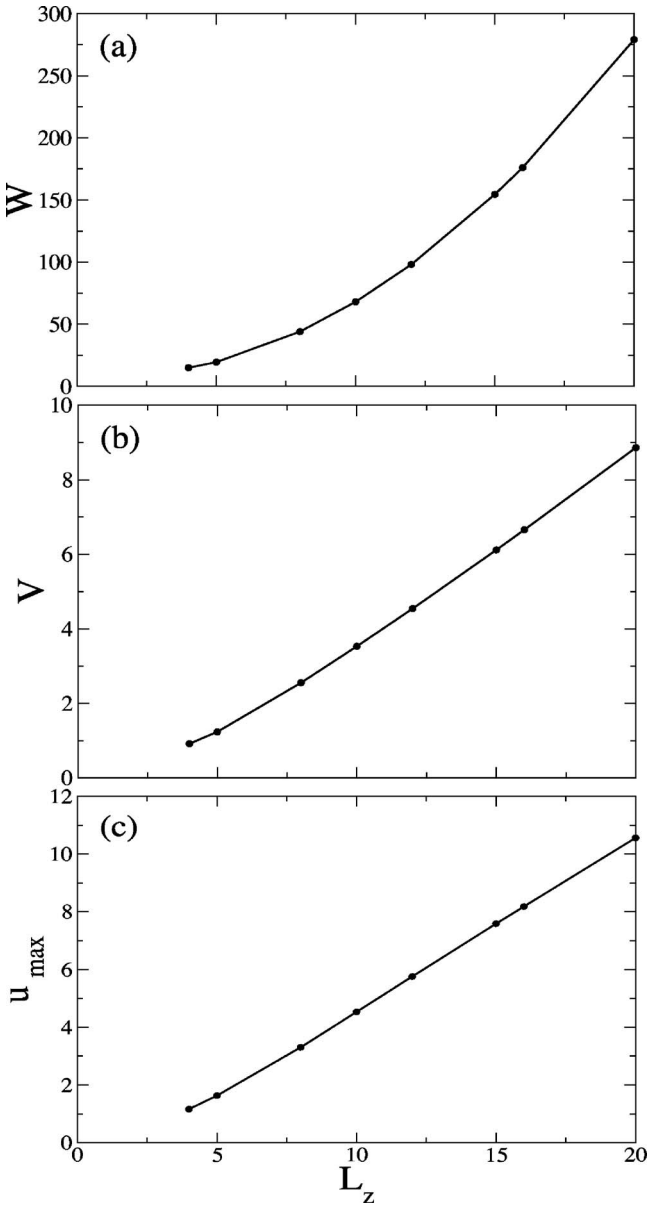

FIG. 9. Asymptotic mixing length W (a), nonlinear propagation speed V (b), and maximum absolute value $u_{\max}$ of the asymptotic horizontal velocity u (c) as a function of the layer thickness.

boundary conditions at the bottom and at the top when L_z increases. Figure 10 shows the asymptotic profiles of the horizontal fluid velocity u across the layer plotted as a function of the renormalized height and taken at the position $x_{\max}$ along x where $|u|$ is the maximum for the various L_z.

C. Influence of the reaction kinetics

The kinetics we have considered so far, $f(c)=c^2(1-c)$, is a monostable kinetics admitting one stable steady state $c=1$ invading the marginally stable steady state $c=0$ at a RD speed v. Clearly the asymptotic dynamics described for this monostable kinetics has autosimilar properties which suggests that analytical work might be undertaken to better characterize it. Such future work would benefit from checking what happens when the RD base state has zero speed v.

To do so, let us now consider a bistable kinetics $f(c)$

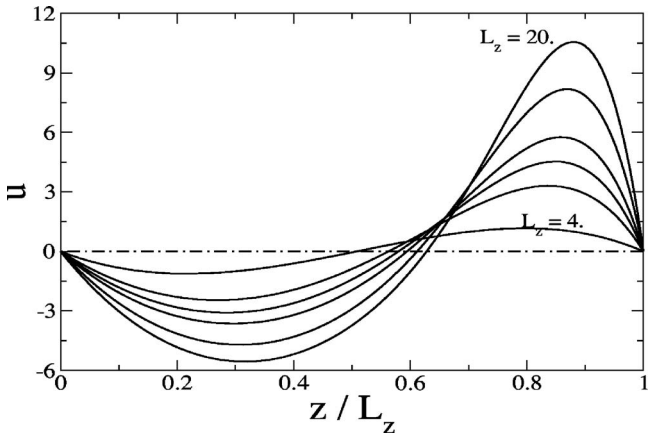

FIG. 10. Horizontal component of the asymptotic fluid flow u measured at $x_{max}=x_{|u|=|u|_{max}}$ as a function of z/L_z for various values of the layer thickness, $L_z=4;8;10;12;16;20$. The dot-dashed curve corresponds to the no-flow situation.

$=c(1-c)(c-d)$, where d is a kinetic parameter, $0<d<1$. This bistable reaction scheme admits two kinetically stable steady states $c=0$ and $c=1$, and one unstable steady state $c=d$. Note that when $d=0$, we recover the monostable kinetics previously studied in Secs. III A and III B. In the absence of convection, the bistable chemical RD front connecting the two stable steady states has the same analytical form (10) as for the monostable kinetics but with a propagation speed v given now by $v=\sqrt{2}/2(1-2d)$. The parameter d controls the relative stability of the two stable steady states: if $d<1/2$, $c=1$ is the most stable one and invades $c=0$ with a positive propagation speed v, and conversely for $d>1/2$. Most importantly, for $d=1/2$, the two steady states are equistable and the propagation speed of the front connecting them is zero. This particular case corresponds to a motionless reaction-diffusion base state.

For $d\neq 1/2$, the effect of chemically induced buoyancy convection on the bistable front is qualitatively similar to the monostable case, i.e., we recover a fluid vortex surrounding the front, stretching, and accelerating it. As the initial condition is the same as for the monostable kinetics ($c=1$ to the left of $c=0$), the vortex turns clockwise if the Rayleigh number is positive and counterclockwise for negative Ra. As for the monostable kinetics, let us focus on positive Ra, as the situation for negative Ra can be obtained by symmetry.

When $c=1$ invades $c=0$ to the right for $d<1/2$, the maximum u intensity u_{max} corresponds to a positive horizontal fluid velocity u and is localized in the upper part of the layer. On the other hand, when $c=0$ invades $c=1$ to the left for $d>1/2$, u_{max} corresponds to a negative u localized in the lower part of the layer. We can therefore conclude that u is always maximum in the direction of the front propagation, which is coherent with the observations made for the monostable case, where u_{max} and the propagation speed are always positive.

Let us now focus on the particular value $d=1/2$. The initial condition corresponds then to the immobile RD front that we position in the middle of the box and we choose a Rayleigh number, Ra=100, and a layer thickness, $L_z=10$.

Figure 11 shows that, in the presence of convection, the bistable front is deformed around its initial position to reach an asymptotic shape with a constant mixing length $W=208.5$ but that it does not propagate so that the steady reaction-diffusion-convection regime corresponds to a standing front surrounded by a fluid vortex. This solution is symmetric with respect to the transformation $x\rightarrow -x$, $z\rightarrow -z$, $c\rightarrow 1-c$, $(u,w)\rightarrow(-u,-w)$. As for the monostable kinetics, the return flow is asymmetric across the layer except for one position along x which corresponds here to the initial position of the front, here $x=L_x/2$. The maximum u intensity u_{max} is also localized at this position and corresponds to a positive and a negative u localized, respectively, in the upper and lower parts of the layer, symmetrically with respect to $z=0$. Moreover, we note that, for the same values of Ra and L_z, the convective motions are less important in the bistable case than in the monostable one but the deformation of the front is more pronounced. The nonpropagating steady vortex shown in Fig. 11 for the bistable kinetics would be a good starting candidate to investigate analytically the nonlinear solutions of the RDC equations. (4)–(9).

D. Comparison with experiments

The interest of the monostable kinetics $f(c)=c^2(1-c)$ is that it is a good quantitative model for the effective kinetics of the iodate-arsenous acid (IAA) reaction in some concentration ranges. Indeed, the detailed kinetics of this autocatalytic redox reaction has been shown to reduce to the one-variable cubic monostable kinetics $f(c)=c^2(1-c)$, with c being the dimensionless concentration of I^- when the arsenous acid is in excess.[31–33] This is the case for experimental results by Pojman *et al.* in their study of the influence of buoyancy convection on the propagation of IAA fronts in capillary tubes.[11] The products of this reaction are lighter than the reactants with $d\rho/d[I^-]=-1.7\times 10^{-2}$ g/cm^3 M which, using the other parameters given in the paper, corresponds to a positive value of the Rayleigh number Ra=0.2. In Table 4 of the article by Pojman *et al.*,[11] the front velocity dependence on the tube radius is given for ascending, descending, and horizontal fronts. As the products are lighter than the reactants, both ascending and horizontal fronts are unstable in the gravity field and therefore propagate at velocities affected by convection. In contrast, descending front

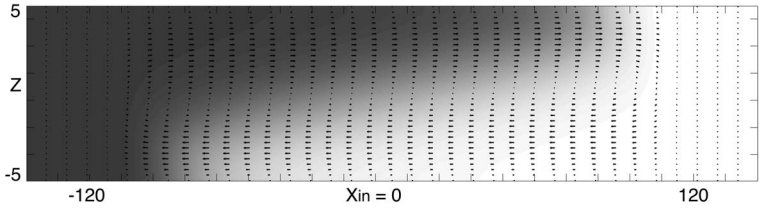

FIG. 11. Focus on the asymptotic convection roll traveling with the deformed bistable front for Ra=100 and $L_z=10$. The z direction is magnified compared to the x direction, see caption of Fig. 3.

TABLE I. Comparison between experimental and numerical propagation speeds for different tube radii. The experimental values have been obtained from Pojman *et al.* (Ref. 11) and the numerical integrations have been performed with Ra=0.2 computed with $d\rho/dc=-1.7\times10^{-2}$ g/cm^3 M, $a_0=5$ mM, $L_c=7.7\times10^{-3}$ cm, $g=980$ cm/s^2, $\mu=0.0089$ g/cm s, and $D=2.04\times10^{-5}$ cm^2/s.

	$10^3\times$ velocity (cm/s)	
Tube radius (cm)	Expt.	Numerical
0.047	3.35	3.24
0.089	4.70	4.84
0.12	5.83	6.44

corresponds to a stable stratification of the light products on top of the heavier reactants and therefore propagates at a constant dimensional reaction-diffusion speed $v_{expt}\approx2.97\times10^{-3}$ cm/s. As the dimensionless RD speed $v=\sqrt{2}/2$, we can calculate the value of the characteristic velocity $U_c=v_{expt}/v$ we have used to nondimensionalize our equations. Here, $U_c=4.2\times10^{-3}$ cm/s for the reaction mixture studied by Pojman *et al.*[11] In the same way, the typical width of an IAA front is more or less equal to 1 mm (Ref. 31) while its dimensionless width is given by $2\sqrt{2}\ln 99$. It follows that the characteristic length scale $L_c=7.7\times10^{-3}$ cm. Using L_c and U_c to switch between dimensional variables and dimensionless ones ($L_z=2r/L_c$), where r is the radius of the tube, we obtain the results presented in Table I which compare fairly well with experiments. Note that we have here only taken the solutal density changes into account in our model whereas the IAA reaction is slightly exothermic. If heat effects are included, the total density difference during the reaction amounts to[11] $\Delta\rho=-1.6\times10^{-4}$ g/cm^3, which gives a Rayleigh number Ra=0.4. However, if we use this value of Ra, the propagation speed obtained numerically is far too large which allows us to confirm that thermal density changes are negligible for the IAA reaction[13,30] in the small capillary tubes used by Pojman *et al.* This can be understood since the capillary tubes are so small, all the heat produced in the front is dissipated instantaneously. This illustrates the usefulness of a theoretical approach since in experiments, it is not easy to distinguish thermal effects from solutal effects.

E. Discussion

The interaction between a propagating autocatalytic chemical front and buoyancy-driven convection due to a density difference across the front leads to an asymptotic regime characterized by a steady fluid vortex around the deformed chemical front propagating at a constant RDC speed V larger than the RD speed v. This is drastically different from the pure hydrodynamic situation in which a density difference across a vertical interface leads to convection mixing of the two miscible fluids until a homogeneous solution is reached in the bounded system. In our case, the chemical reaction which is itself at the source of the density gradient localizes the source of convection in the system and gives rise to a localized asymptotic structure by providing a self-sustained moving interface across the two miscible fluids, i.e., the products and reactants.

We can compare this asymptotic dynamics with results obtained for pure Marangoni convection around isothermal chemical fronts studied previously in the absence of gravity.[9,10] In that case, the gradient of surface tension across the front triggers Marangoni flows deforming and accelerating the front. The system reaches a steady regime too, characterized by a convection roll traveling with the chemical front at a constant speed. In that system, the intensity of the coupling between reaction-diffusion processes and convection is quantified by a solutal Marangoni number M. In both situations, the time needed to reach the steady regime is an increasing function of the layer thickness while it is independent of, respectively, the Rayleigh number and the Marangoni number. We have also observed that the characteristics of the asymptotic regime, i.e., the mixing length W, propagation speed V, and maximum horizontal velocity u_{max}, are increasing functions of both the Rayleigh and the Marangoni numbers which can be fitted by a square root function of these numbers at large Ra and M. However, larger Marangoni numbers are needed to achieve same values of W, V, and u_{max}.

An important difference between Marangoni and buoyancy-driven convection traveling with chemical fronts is the behavior for negative Ra and M. While the situation at negative Rayleigh number can be obtained by symmetry with regard to the positive Ra case, there is an asymmetry between the results for positive and negative Marangoni numbers. This is due to the fact that the flow initiated at the surface by Marangoni effect is, respectively, parallel ($M>0$) or antiparallel ($M<0$) to the front propagation.

Following this, in the case of pure Marangoni convection, the maximum u intensity u_{max} is always located at the surface but corresponds to, respectively, positive and negative u depending whether $M>0$ or $M<0$. On the other hand, in the case of pure buoyancy convection, the sign of u_{max} is the same as the sign of the front propagation speed, typically positive for the monostable kinetics studied with our specific initial condition. Therefore, it is located in the upper part of the layer for positive Ra while it is shifted to the lower part for negative Ra.

Another comparison point concerns the return flow across the layer. Marangoni return flows are asymmetric across the layer and get their minimum, zero, and maximum values at the same positions across the layer, i.e., at $L_z/3$, $2L_z/3$, and L_z (surface), independent of M, L_z, M sign, or d (type of kinetics). On the contrary, the asymmetry of buoyancy return flows depends on the layer thickness and on the kinetics while it is independent of Ra. Indeed, there is an autosimilarity of the results observed at large Ra which is also observed for Marangoni dynamics at large M.

The last difference has to do with the bistable kinetics when the two steady states are equistable ($d=1/2$). In this particular case, the reaction-diffusion front has a zero RD speed. Buoyancy effects deform this front but do not affect the relative stability of the two stable states so that the reaction-diffusion-convection solution is a nonpropagating front surrounded by a steady fluid vortex. By contrast, Ma-

rangoni effects change the effective stability of the two steady states and make the front and the surrounding vortex propagate.[40]

Finally, we have performed a linear stability analysis of the steady buoyancy-driven two-dimensional base state shown in Fig. 3 with regard to periodic spanwise perturbations and the asymptotic reactive vortex has been found stable.

IV. CONCLUSIONS

When two nonreactive miscible fluids of different density are brought into contact in a horizontal thin closed system, the vertical interface between them is always unstable with regard to mixing due to the fact that the heavier solution sinks below the lighter one. Autocatalytic traveling fronts provide a simple model system to analyze to what extent the presence of a chemical reaction at the source of the density gradient can modify this picture. By numerically integrating a reaction-diffusion-convection model for the concentration of the product of an autocatalytic reaction coupled to the incompressible Stokes equations for the flow, we show that the coupling between hydrodynamics and reaction-diffusion processes leads here to one single localized vortex surrounding the front and deforming it.[30] In the presence of this localized fluid flow, the speed of the RDC front V is larger than the speed v of the RD planar front. We have here characterized both the transient and asymptotic dynamics around the convective fronts by a followup in time of the concentration and velocity fields as well as of the properties of their averaged transverse and longitudinal profiles. Measurements of the dependence of the asymptotic mixing length W, of the RDC speed V, and of the maximum speed $u_{\max}$ in the system have been provided as a function of both the Rayleigh number Ra and the height L_z of the system. We find, in particular, that W and V scale as $\sqrt{\mathrm{Ra}}$ for $\mathrm{Ra} > 5$. A further characterization of the flow field in the depth of the layer and of depth-averaged concentration profiles evidences self-similarity properties of the RDC dynamics. Comparison with data on the speed of deformed IAA fronts traveling in horizontal capillary tubes[11] shows encouraging agreement. Further detailed experimental data on the influence of density variations across the front (obtained, for instance, through concentration changes) and of the layer thickness on the properties of the deformed front would be welcome.

We have furthermore described the convective deformation of chemical fronts in the case of a bistable kinetics which provides results interesting to be used for further analytical studies of the nonlinear properties of RDC systems. Eventually, we have also provided a comparison of the dynamics and of the important scalings of the pure buoyancy-driven chemohydrodynamic flows studied here with those previously studied in the case of pure Marangoni-driven spatiotemporal dynamics.[9,10]

The present work has considered isothermal fronts as a first step. In this case, the density jump across the front is only due to a solutal contribution $\Delta\rho_s$ related to compositional changes in the course of reaction. It would be interesting to consider in further work the influence of heat effects in exothermic reactions which will bring in an additional thermal contribution $\Delta\rho_T$ to the density jump.[6] The fact that heat diffuses more rapidly than mass and also the possible competition between antagonistic solutal and thermal buoyancy effects is expected to lead to interesting new dynamics as is the case for fronts traveling in vertical geometries.[20,21] In parallel, this work complements our previous studies[9,10] of the influence of pure Marangoni stresses on the deformation and acceleration of fronts traveling in horizontal layers open to the air but in the absence of gravity. In practice, in such geometries, Marangoni and buoyancy effects will most often both be present. In this respect, it would be interesting to complement these previous and present studies by a theoretical analysis of the RDC dynamics of fronts when both Marangoni and buoyancy effects act at the same time. This would allow to give interesting information for experimentalists analyzing dynamics of fronts in thin solution layers open to the air, for instance. It might, in particular, allow to understand complicated flows and front deformations observed experimentally in the past and which clearly result from intricate combination of surface-tension and buoyancy-driven effects.[4,6–8]

ACKNOWLEDGMENTS

L.R. is supported by a FNRS (Belgium) PhD fellowship. A.D.W. acknowledges financial support from Prodex (Belgium), FNRS and from the "Communauté Française de Belgique" ("Actions de Recherches Concertées" Programme).

[1] I. R. Epstein and J. A. Pojman, *An Introduction to Nonlinear Chemical Dynamics* (Oxford University Press, Oxford, 1998).
[2] T. A. Gribschaw, K. Showalter, D. L. Banville, and I. R. Epstein, J. Phys. Chem. **85**, 2152 (1981).
[3] G. Bazsa and I. R. Epstein, J. Phys. Chem. **89**, 3050 (1985).
[4] I. Nagypal, G. Bazsa, and I. R. Epstein, J. Am. Chem. Soc. **108**, 3635 (1986).
[5] H. Miike, S. C. Müller, and B. Hess, Chem. Phys. Lett. **144**, 515 (1988).
[6] J. A. Pojman and I. R. Epstein, J. Phys. Chem. **94**, 4966 (1990).
[7] M. J. B. Hauser and R. H. Simoyi, Phys. Lett. A **191**, 31 (1994); M. J. B. Hauser and R. H. Simoyi, Chem. Phys. Lett. **227**, 593 (1994).
[8] B. S. Martincigh and R. H. Simoyi, J. Phys. Chem. **106**, 482 (2002).
[9] L. Rongy and A. De Wit, J. Chem. Phys. **124**, 164705 (2006).
[10] L. Rongy and A. De Wit, J. Eng. Math. (in press).
[11] J. A. Pojman, I. R. Epstein, T. J. McManus, and K. Showalter, J. Phys. Chem. **95**, 1299 (1991).
[12] I. P. Nagy, A. Keresztessy, J. A. Pojman, G. Bazsa, and Z. Noszticzius, J. Phys. Chem. **98**, 6030 (1994).
[13] J. Masere, D. A. Vasquez, B. F. Edwards, J. W. Wilder, and K. Showalter, J. Phys. Chem. **98**, 6505 (1994).
[14] A. Keresztessy, I. P. Nagy, G. Bazsa, and J. A. Pojman, J. Phys. Chem. **99**, 5379 (1995).
[15] M. Böckmann and S. C. Müller, Phys. Rev. Lett. **85**, 2506 (2000).
[16] D. Horváth, T. Bánsági, Jr., and A. Tóth, J. Chem. Phys. **117**, 4399 (2002).
[17] R. Demuth and E. Meiburg, Phys. Fluids **15**, 597 (2003).
[18] A. De Wit, Phys. Fluids **16**, 163 (2004).
[19] M. C. Rogers and S. W. Morris, Phys. Rev. Lett. **95**, 024505 (2005).
[20] J. D'Hernoncourt, A. Zebib, and A. De Wit, Phys. Rev. Lett. **96**, 154501 (2006); Chaos **17**, 013109 (2007).
[21] J. D'Hernoncourt, A. De Wit, and A. Zebib, J. Fluid Mech. **576**, 445 (2007).
[22] C. Haertel, E. Meiburg, and F. Necker, J. Fluid Mech. **418**, 189 (2000).
[23] J. E. Simpson, *Gravity Currents in the Environment and the Laboratory*, 2nd ed. (Cambridge University Press, Cambridge, 1997).
[24] H. Wilke, Physica D **86**, 508 (1995).
[25] Y. Wu, D. A. Vasquez, B. F. Edwards, and J. W. Wilder, Phys. Rev. E **51**,

1119 (1995).
[26] K. Matthiessen and S. C. Müller, Phys. Rev. E **52**, 492 (1995).
[27] K. Matthiessen, H. Wilke, and S. C. Müller, Phys. Rev. E **53**, 6056 (1996).
[28] M. Diewald, K. Matthiessen, S. C. Müller, and H. R. Brand, Phys. Rev. Lett. **77**, 4466 (1996).
[29] V. Pérez-Villar, A. P. Muñuzuri, and V. Pérez-Muñuzuri, Phys. Rev. E **61**, 3771 (2000).
[30] D. A. Vasquez, J. M. Littley, J. W. Wilder, and B. F. Edwards, Phys. Rev. E **50**, 280 (1994).
[31] A. Hanna, A. Saul, and K. Showalter, J. Am. Chem. Soc. **104**, 3838 (1982).
[32] *Oscillations and Traveling Waves in Chemical Systems*, edited by R. J. Field and M. Burger (Wiley, New York, 1985).
[33] K. Showalter, in *Kinetics of Nonhomogenous Processes*, edited be G. R. Freeman (Wiley, New York, 1987), p. 769.
[34] A. Wray, report, 1991 (unpublished).
[35] S. K. Lele, J. Comput. Phys. **103**, 16 (1992).
[36] D. Gottlieb and S. A. Orszag, *Numerical Analysis of Spectral Methods* (SIAM, Philadelphia, PA, 1977).
[37] C. Canuto, M. Y. Hussaini, A. Quarteroni, and T. A. Zang, *Spectral Methods in Fluid Mechanics* (Springer, New York, 1988).
[38] C. A. J. Fletcher, *Computational Techniques for Fluid Dynamics* (Springer, New York, 1991), Vol. 1.
[39] N. Goyal and E. Meiburg, J. Fluid Mech. **516**, 211 (2004).
[40] L. Rongy and A. De Wit (unpublished).